ChemistrySelect

Research Article
doi.org/10.1002/slct.202400054

Chemistry Europe
European Chemical Societies Publishing

www.chemistryselect.org

5-Bromosalicylaldehyde: Theoretical, Experimental and Spectroscopic (FT-IR, Raman, H^1 and C^{13}-NMR, UV-Vis) Studies and Their Photovoltaic Parameters

Semiha Bahçeli,[a] Ebru Karakaş Sarıkaya,*[b] and Ömer Dereli[c]

This study aims to identify a 5-bromosalicylaldehyde (5BSA) and assess its performance for application in organic solar cells. In the current work, the 5BSA was investigated using various techniques such as FT-IR, Raman, NMR, and UV-Vis spectroscopy to characterize the title molecule. The possible conformers of the 5BSA were studied using the MMFF methodology in Spartan software. The geometry optimization of modifications for each conformation was computed using the DFT approach for the B3LYP/6-311++G(d,p) functional. The energy and dipole moment of most stable form were determined −1879057.42 kcal/mol and 1.455 Debye, respectively. The FT-IR and Raman vibrational frequencies, the H^1 and C^{13} NMR chemical shift values (in vacuum and in DMSO-d_6), the UV spectrum calculations (both in vacuum and in the solvent ethanol), the HOMO-LUMO energy, and the map of MEP. Meanwhile, by considering the properties of organic photovoltaic cells, the open-circuit voltage (V_{OC}), hole reorganization energy (λ_h) and electron reorganization energy (λ_e), light-harvesting efficiency (*LHE*), total reorganization energy (λ_{total}), the short-circuit current density (J_{sc}), the driving force (ΔG_{inject}), binding energy (E_b) were also computed for the title compound. In addition, transition density matrix (TDM) and density of states (DOS) analyses were conducted for the 5BSA molecule.

Introduction

In recent years, organic molecules are widely researched because of their affordability, simple synthesis, and ease of production. Simple alterations to the structure of organic compounds allow for adjusting their chemical structure and characteristics to achieve specific non-linear optical properties.[1] Moreover, molecular materials have attracted considerable attention due to their potential applications in novel optoelectronic devices. The conducting and optical properties of organic compounds have been the subject of intense research activity. The reason for the focus on organic compounds is the many advantages they possess compared to inorganic structures with respect to optoelectronic device applications.[2]

The density functional theory (DFT) has garnered considerable attention in the field of current chemistry due to its ability to accurately simulate specific chemical processes and the energy of the system. Consequently, it has emerged as a prominent instrument for theoretical research. Calculations utilizing DFT play a crucial role in providing important insights into several aspects of chemical reactions, including reaction mechanisms, stability analysis, identification of reactive sites, characterization of electronic properties, and determination of structural attributes.[3] Theoretical chemists can derive equations that allow the calculation of molecular properties based on the macroscopic and microscopic attributes of different groupings of molecules. Unique modifications to electrical properties can be achieved by altering the contributing and accepting groups.[4]

On the other hand, in recent years, organic photovoltaic cells have become the focus of great interest in organic materials, such as solar cells.[5] Organic solar devices have emerged as a crucial class of photovoltaic devices[6] because of their advantageous attributes, including a simplified fabrication method and use of organic materials. In addition, conjugated molecules have favorable characteristics for the generating significant photocurrent.[7] Hence, a comprehensive understanding of E_{LUMO}, E_{HOMO}, and E_{gap} is essential to conduct a thorough examination of the impact of electron-releasing and electron-accepting groups on the attachment of these groups to the compound under investigation.[5] Furthermore, the discrepancy in energy levels between the highest-energy occupied molecular orbital (HOMO) and the lowest-energy unoccupied molecular orbital (LUMO) is important in determining the electrical transport characteristics of a molecule. The examination of the energy values associated with HOMO and LUMO might aid the collection of molecular characteristics. Moreover, HOMO and LUMO are closely linked to the ionization potential and electron affinity of the molecule. The electron-donating characteristics, electron-accepting characteristics, and stability of the molecule can be ascribed to the disparity in energy levels between HOMO and LUMO. The energies associated with the HOMO and LUMO play a pivotal role in radical processes.[7,8]

[a] *Prof. Dr. S. Bahçeli*
Department of Astronautical Engineering, Turkish Aeronautical Association, Bahçekapı Mah. Okul Sk. No:11, 06790 Etimesgut, Ankara, Turkey

[b] *Asst. Prof. Dr. E. K. Sarıkaya*
Department of Engineering, Necmettin Erbakan University, Köyceğiz Mah. Demeç Sk. No:44/1, 42090 Meram, Konya, Turkey
E-mail: eksarikaya@erbakan.edu.tr

[c] *Prof. Dr. Ö. Dereli*
Department of Education, Necmettin Erbakan University, Aşkan Mah. Meram Yeni Yol Sk. No:132, 42090 Meram, Konya, Turkey

In this framework, the investigation of the relationship between a molecule's structure and its activity is anticipated to be most effectively conducted using the Molecular Electrostatic Potential (MEP), which is often regarded as the foremost electrostatic attribute of significance. The utilization of this technique seems to be useful in elucidating several chemical and physical phenomena within the realm of chemistry. The examination of molecular interactions can be facilitated by utilizing MEP, because it is directly linked to the overall charge distribution of a molecule. The utilization of a molecule's MEP enables the assessment and prediction of relative positions for electrophilic and nucleophilic assault, and hydrogen bonding interactions. This study elucidates the interconnections among chemical reactivity, electron negativity, dipole moments, and partial charges exhibited by molecules.[5,9]

To the best of our knowledge, there is no study on 5BSA in terms of spectroscopic, DFT calculation, and photovoltaic parameters in the literature. For this reason, we found the mentioned compound to be worth investigating. In the present work, we report both experimental and theoretical results of the FT-IR and Raman vibrational wavenumbers, proton and carbon-13 NMR chemical shift values, UV-vis maximum wavelengths, DOS, TDM and computed photovoltaic parameters calculated at the B3LYP/611++G(d,p)[10] level.

Experimental

5BSA was utilized after being acquired from international wholesalers (such Merck or Aldrich). The IR spectrum of solid 5BSA was recorded in the range 3500–500 cm^{-1} on Thermo Nicolet™ iS50 IR Spectrometer at room temperature. Raman spectrum was obtained from the Nd: YAG laser in the Brucker FRA 106/S spectrometer. The Raman spectrum was recorded by applying laser irradiation at 785 nm and 30 mW power in the wavelength range of 3500–500 cm^{-1}. Tetramethyl silane (TMS) was used as an inner benchmark when measuring ^{1}H NMR spectra on a Varian 400 MHz spectrometer, and ^{13}C NMR spectra were collected from measurements of a Varian (400–100 MHz) spectrometer in dimethyl sulfoxide-d6 (DMSO-d6). Chemical shifts are expressed in ppm. The UV absorbance spectrum of the 5BSA molecule solved in ethanol was obtained in the 200–400 nm region using a Shimadu UV-300 Plus spectrophotometer.

Computational Details

A definite structure between possible structures is investigated by theoretical computations. In order to do this, the initial task is to create conformers by scanning the potential energy region. To determine the correct structure, the calculations began with conformational analysis. The Spartan 14 program[11] was used for conformational analysis, and the conformational space of molecules were scanned using the Molecular Mechanics Force Fields (MMFF)[12] method. For theoretical calculations, we gave ten-degree rotations to the sigma bonds (C4–C10 and C5–O2) of the compound. Thanks to these computations, four conformations of 5BSA were found.

Then, 5BSA geometry was optimized using DFT/B3LYP[13] techniques using 6–311++G(d,p)[10]. Default settings have been used. The conformations with overlapping energy were removed from the computations using Gaussian software.[14] The conformation with the lowest energy was identified as the structure most likely to be found in nature by comparing the conformational energies. The output files were visualized using Gauss View 5[15] software. A definite structure between possible structures is searched for through theoretical computations. In order to do this, the first step is to create conformers by scanning the potential energy region. Calculations were performed in ground state.

FT-IR and Raman vibrations were found both theoretically and experimentally. DFT was used to perform research on infrared and Raman properties while comparing theoretical predictions with experimental findings. After determining the geometrical optimization for a stable conformer, vibrational frequency calculations were performed for the optimized structural parameters of this conformer. FT-IR and Raman computations of the molecule were calculated using DFT/B3LYP with 6–311++G(d,p) basis set in the ground state. Nevertheless, the wavenumber values obtained at the stated level are subject to widely recognized systematic inaccuracies. In order to mitigate the well-recognized systematic errors, the vibrational wavenumbers obtained by computation at the B3LYP/6-311++G(d,p) level of theory were subjected to scaling factors of 0.967 (for wavenumbers below 1800 cm^{-1}) and 0.955 (for wavenumbers beyond 1800 cm^{-1}).[16]

Isotropic chemical shifts are often employed to help in the identification of organic compounds, and to obtain reliable studies of magnetic properties, accurate predictions of molecular geometries are necessary. For calculating nuclear magnetic shielding tensors, the GIAO[17] method is one of the most commonly applied approaches, and the B3LYP method helps in calculating the shielding constants with accuracy. We calculated the ^{1}H and ^{13}C NMR isotropic shielding employing the GIAO method by means of the optimized parameters obtained from B3LYP/6-311++G(d,p) method. We also included the impact of the solvent (DMSO) on the theoretical NMR parameters using the default model IEF-PCM supplied by Gaussian 09.[14]

MEP calculations for the 5BSA molecule were carried out at the B3LYP/6-311++G(d,p) level. MEP in three-dimensional (3D) was performed using the Gauss View 5[15] program. Furthermore, the MEP figure demonstrates the electrostatic potentials at the surfaces represented by blue, red, and green. In this content, the regions of negative and positive electrostatic potentials are represented by red and blue parts, respectively, and the regions with zero potentials are indicated by green. Meanwhile, it can be reminded that the electrophilic reactivity is related to the negative regions of the MEP whereas the nucleophilic reactivity is related to the positive ones. Parameters such as E_{LUMO}, E_{HOMO}, and E_{gap} play a crucial role in assessing the feasibility of charge transfer between the acceptor and donor entities. Moreover, it should be noted that these factors have a strong correlation with the performance and photovoltaic characteristics of solar cells. With the obtained and calculated values of E_{LUMO}, E_{HOMO}, and E_{gap}, they are used to further investigate chemical reactivity indices such as chemical potential (μ), electronegativity (χ) and chemical hardness (η).[18] Theoretical DFT-TD calculations provide a more accurate explanation of the absorption properties of the compound under investigation and might be recommended for determining the electronic features of other materials. All of these parameters were calculated and computed using the DFT-TD[19]/B3LYP method and 6–311++G(d,p) basis set in this study. To figure out the energy, we used DFT theory with B3LYP/6-311++G(d,p) to look at the excited state time-dependent self-consistent field (TD-SCF) of 5BSA in both the gaseous and solvent phases.

In the context of a solar cell, the semiconductor material experiences the phenomenon of light absorption, resulting in the

creation of electron-hole pairs. These pairs are then separated by the internal electric field present within the cell, thus enabling the establishment of an electrical current. The efficacy of this strategy is contingent on the accessibility and mobility of charge carriers without cost. The examination of the DOS provides insights into the energy levels of the semiconductor material and the corresponding densities of states. Understanding this information is of utmost importance in determining the energy required for the generation of electron-hole pairs and the energy necessary for their subsequent recombination. The measurement of density of states (DOS) provides additional assistance in understanding the mechanisms involved in charge transfer and recombination inside cells.[20] DOS was estimated with the DFT-TD method, and a curve plot was obtained using the PyMOlyze 1.1[21] package. Another technique for evaluating the exciton's creation, mobility, and separation is TDM analysis. The calculation of TDM energy was performed utilizing TD-DFT/B3LYP/6-311++G(d,p) and the Multiwavefunction 3.8[22] (two-dimensional) program to generate a colored plot.

Results and Discussion

Geometry and Optimization

The findings of molecular geometry showed that the 5BSA molecule has four stable conformers in the solid state, as shown in Figure 1.

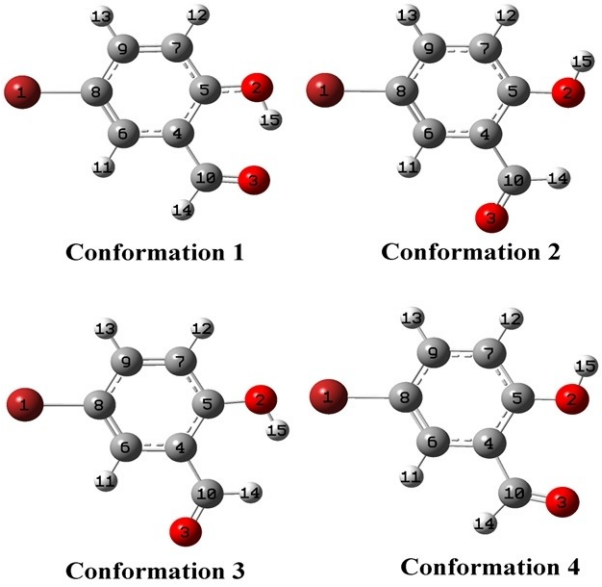

Figure 1. Four conformers of 5BSA molecule.

Table 1. The energies and dipole moments of the 5BSA molecule.

Conf.	E (kcal/mol)	ΔE (kcal/mol)	Dipole Moment (Debye)	Boltzmann Distribution
1	−879037960.88	0.00	1.455	100,00 %
2	−879029816.52	8.14	5.288	0,00 %
3	−879028391.46	9.57	2.919	0,00 %
4	−879026983.34	10.98	3.530	0,00 %

Figure 1 presents the molecular composition of the conformers and the technique for numbering the atoms. Table 1 presents the conformational energy, energy difference, and Boltzmann Distribution of the conformers. Four distinct conformers of 5BSA have been found by conformational analysis calculations. Given that our calculations were conducted under standard room temperature conditions and the energy disparity between the two conformers exceeds 5 kcal/mol, it may be inferred, in accordance with the principles of the Boltzmann distribution, that only conformer 1 is thermodynamically favored and likely to be present at room temperature.

As a result, Table 2 lists the optimized molecular geometric parameters at the DFT/ B3LYP level.

A comparison of theoretical and experimental measurements of the Raman spectrum in Figure 3.

FT-IR-RAMAN Analysis

The 5BSA molecule has 15 atoms and 39 normal vibrational modes. Infrared and Raman are active in all modes of the molecule. The assignment of bands observed in the solid-state FT-IR and Raman spectra of the 5BSA was supported by theoretical calculations. Frequencies are calculated in harmonic approximation using B3LYP/6-311++G(d,p)[23] basis set. The comparison of the theoretically calculated and experimentally recorded FT-IR and Raman spectra of the 5BSA molecule is shown in Figures 2 and 3, respectively. Experimental and calculated vibration frequencies are compared in Table 3. Then, the vibrational movements of various atomic groups corresponding to the frequency values of these vibrational modes were evaluated. Experimental and computed FT-IR spectra were shown in Figure 2.

The C–H stretching vibration in the organic compounds is in the characteristic band region of 3100–3000 cm^{-1}.[24] A weak band was observed at 3065 cm^{-1} in FT-IR spectrum and the band which was observed at 3067 cm^{-1} in Raman spectrum assigned to the C–H symmetric stretching vibrations, and the theoretically predicted value 3061 and 3048 cm^{-1} was assigned to the C–H symmetric and antisymmetric stretching vibrations of 5BSA, respectively. The other C–H stretching vibrations of the 5BSA were observed at 3041, and 2872 cm^{-1} in FT-IR spectrum and at 3043, and 2880 cm^{-1} in Raman spectrum. The theoretical counterpart of these band was seen at 3039 and 2820 cm^{-1}. The in-plane C–H bending vibrations of rings were observed at 1460, 1340, 1208, 1163, 1114, and 1053 cm^{-1} in FT-IR spectrum and the bands at 1467, 1209, 1155, 1115 and 1069 cm^{-1} in Raman spectrum (mode nos.: 9, 12, 15, 16, 17, 18). In the Table 4, the band observed at 975, and 828 cm^{-1} in FT-IR spectrum and 956, and 831 cm^{-1} in Raman spectrum was assigned as C–H out of plane bending vibration. The theoretically computed wavenumbers for this vibrations are 985, 943, 862 and 816 cm^{-1}.

Two different type CO stretching vibrations are observed at 5BSA. The first one is C=O (double bond) and the second one is C–O (single bond) stretching vibrations. The C=O stretching frequency appears strongly in the infrared spectrum in the

Table 2. The bond lengths (*A*), bond angles (^{0}), and dihedral angles (^{0}) of the conformations of the 5BSA molecule calculated using the B3LYP/6-311++G(d,p) basis set.

Bond Lengths	Conf1	Bond Lengths	Conf1	Bond Angles	Conf1	Bond Angles	Conf1	Dihedral Angles	Conf1	Dihedral Angles	Conf1
C10,C4	1.457	C10,C4	1.457	C4,C10,O3	124.0	C9,C7,C5	120.3	H14,C10,C4,C5	180	C9,C8,C6,C4	0.0
C10,O3	1.227	C10,O3	1.227	Br1,C8,C6	120.2	C9,C8,C6	120.3	Br1,C8,C6,C4	−180	C9,C8,C6,H11	−180
C5,C4	1.417	C5,C4	1.417	Br1,C8,C9	119.5	H11,C6,C4	119.3	Br1,C8,C6,H11	0.0	H11,C6,C4,C10	0.0
C5,O2	1.339	C5,O2	1.339	C10,C4,C5	120.4	H11,C6,C8	120.8	C4,C5,O2,H15	0.0	H11,C6,C4,C5	180
C6,C4	1.407	C6,C4	1.407	C10,C4,C6	119.8	H12,C7,C5	118.8	C7,C5,C4,C10	180	H12,C7,C5,C4	−180
C7,C5	1.401	H11,C6	1.084	C4,C10,H14	116.1	H12,C7,C9	120.9	C7,C5,C4,C6	0.0	H12,C7,C5,O2	0.0
C8,Br1	1.916	H12,C7	1.083	C5,O2,H15	108.0	H13,C9,C7	119.8	C7,C5,O2,H15	−180	H13,C9,C7,C5	−180
C8,C6	1.380	H13,C9	1.083	C6,C4,C5	119.8	H13,C9,C8	119.8	C7,C9,C8,Br1	180	H13,C9,C7,H12	0.0
C9,C7	1.386	H14,C10	1.105	C7,C5,C4	119.1	O2,C5,C4	122.1	C7,C9,C8,C6	0.0	H13,C9,C8,Br1	0.0
C9,C8	1.401	H15,O2	0.984	C7,C9,C8	120.4	O2,C5,C7	118.7	C8,C6,C4,C10	−180	H13,C9,C8,C6	180
				C8,C6,C4	120.0	O3,C10,H14	119.8	C8,C6,C4,C5	0.0	H14,C10,C4,C6	0.0
								C8,C9,C7,C5	0.0	O2,C5,C4,C10	0.0
								C8,C9,C7,H12	180	O2,C5,C4,C6	180
								C9,C7,C5,C4	0.0	O3,C10,C4,C5	0.0
								C9,C7,C5,O2	−180	O3,C10,C4,C6	−180

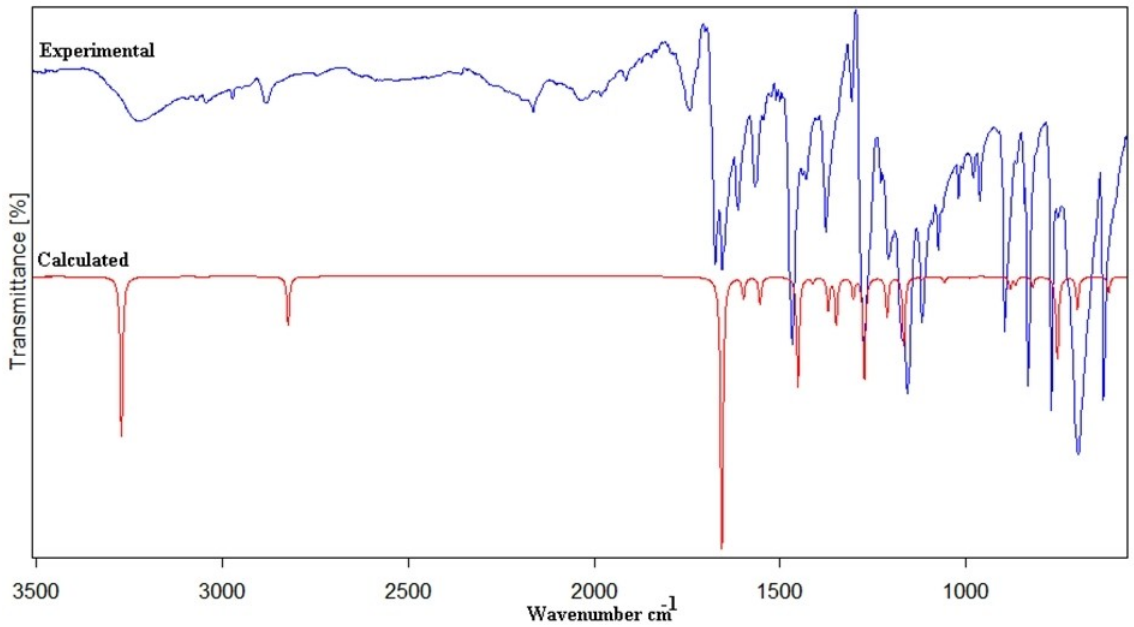

Figure 2. Experimental and theoretical FT-IR spectra of 5BSA molecule.

range 1600–1850 cm^{-1} and C–O stretching vibrations in the range 1100–1300 cm^{-1}.[24a] The strong bands observed at 1650 cm^{-1} in FT-IR spectrum was assigned to the C=O stretching vibrations. The same vibrations were observed at 1655 cm^{-1} in Raman spectrum. The theoretically computed wavenumbers for this vibrations at 1652 cm^{-1}. The values of stretching modes of C–O were 1269 in FT-IR and 1273 cm^{-1} in Raman. The theoretically computed wavenumber for this vibration is 1269 cm^{-1}. In the present work, according to the results of TED analysis, the theoretically predicted value of mode-30 was assigned to the CO in-plane-bending modes. This value is 450 cm^{-1}. Moreover, the theoretically computed wavenumbers for CO out-of-plane bending wavenumbers are 318 cm^{-1}.

The O–H group vibrations are likely to be the most sensitive to the environment, so they show pronounced shifts in the spectra of the hydrogen bonded species.[24a] For the O–H stretching vibrations, the bands observed at 3236 cm^{-1} in FT-IR spectrum and the bands observed at 3271 cm^{-1} in Raman spectrum were assigned to O–H stretching vibrations (mode no 1). The OH in-plane-bending vibrations were observed at, 1371 cm^{-1} in the FT-IR spectrum (mode no 11). The OH in-

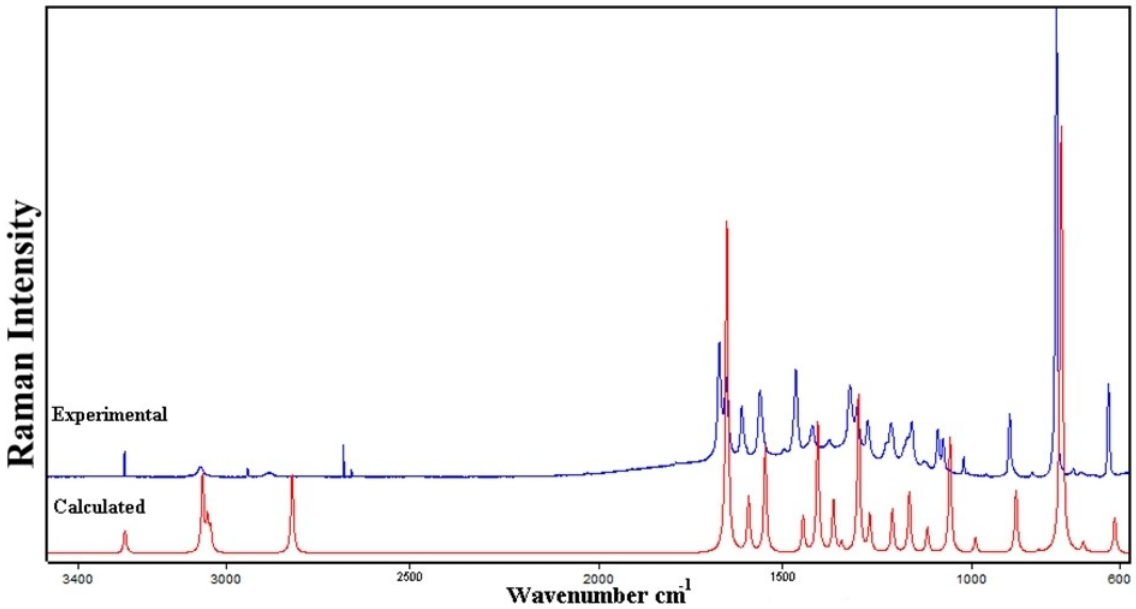

Figure 3. Experimental and theoretical Raman spectra of 5BSA molecule.

plane-bending vibrations were observed at 1379 cm^{-1} in Raman spectrum. The theoretically computed wavenumbers for OH in-plane-bending vibrations at 1366 cm^{-1}. The OH out-of-plane bending wavenumber calculated at 749 cm^{-1} (mode no: 25) using B3LYP/6-311 + + G(d,p) basis set.

NMR Evaluation

In the ^{1}H-NMR spectrum of 5BSA, the Hydrogen protons at 10.92, 10.17, 7.65, 7.56 and 6.93 ppm were observed. The theoretical values of a monomer of 5BSA were found to be higher than the experimental values. Figure 4 displays the trimer structure of the 5BSA molecule. For this reason, dimer and trimer calculations were made considering the hydrogen bonding effect.

As can be seen from the Table 4, the calculated dimer values were found close to the experimental values. Differences are observed in the NMR chemical shifts due to the effect of the Br atom. Both the calculated and experimentally obtained values of ^{13}C-NMR can be seen in the Table 4. As indicated in the table, the calculated dimer values were found close to the experimental values.

Assessment of MEP

The 3D representation of the MEP of the 5BSA compound is presented in Figure 5. Therefore, in our study, Figure 5 shows that the blue sites (positive zones) are localized on the hydrogen atoms of 5BSA whereas the red sites (negative zones) are located on the oxygen atom. On the other hand, the Br atom and ring have some localized zero potentials. Moreover, we employ the calculation of MEP to assess the potential reactivity sites and their respective affinities towards both hard and soft electrophiles and nucleophiles. The main transition at the maximum wavelength is mostly the transition from the H→ L. The nucleophilic zone refers to the area where hydrogen atoms are located, whereas the electrophilic region corresponds to the areas where oxygen atoms are found. The representation of the investigated chemical is color-coded with values that vary from −3.679 e^{-2} (deepest red) through +3.679 e^{-2} (deepest blue).

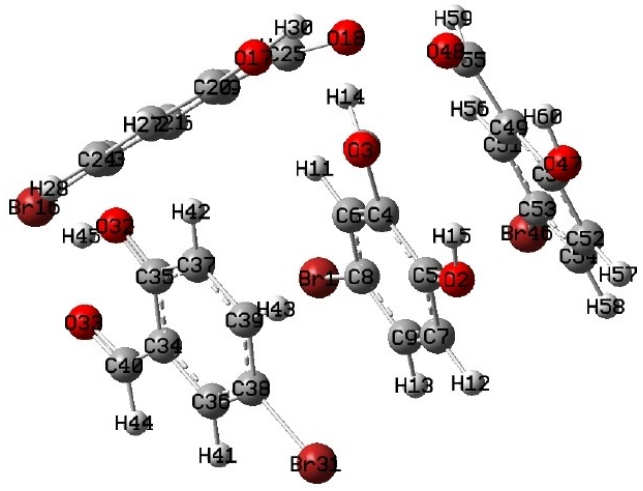

Figure 4. The trimer structure of 5BSA.

Table 3. Comparison of observed and calculated vibration frequencies of 5BSA molecule.

	Experimental		Theoretical			
Mod Num.	FT-IR	FT-Raman	Scaled Freq[a]	I_{FT-IR}	I_{RAMAN}	TED[b] (%)
1	3236	3271	3269	60	10	84 ν(OH)
2	3065	3067	3061	0	33	81 ν_s(CH)
3	-	-	3048	0	13	77 ν_{as} (CH)
4	3041	3043	3040	0	9	74 ν(CH)
5	2872	2880	2820	18	32	78 ν(CH)
6	1650	1655	1653	100	97	19 ν(O=C) + 18 ν(CC) + 17 δ(CCH) + 14 δ(CCC)
7	1598	1612	1594	8	16	31 ν(CC) + 22 δ(CCH) + 16 δ(CCC)
8	1558	1562	1550	10	30	28 ν(CC) + 22 δ(CCH) + 11 δ(CCC)
9	1460	1467	1448	41	10	45 δ(CCH) + 19 ν(CC)
10	1415	1419	1409	2	36	24 ν(CC) + 19 δ(CCH) + 11 δ(CCC)
11	1371	1379	1366	12	14	28 δ(CCH) + 21 ν(CC) + 14 δ(OCH) + 12 δ(COH)
12	1340	-	1344	17	3	39 δ(CCH) + 16 ν(CC) + 10 δ(OCH)
13	1304	1304	1299	7	42	39 ν(CC) + 29 δ(CCH)
14	1269	1273	1269	38	10	28 δ(CCH) + 20 δ(CCC) + 17 ν(CC) + 11 ν(OC)
15	1208	1209	1208	15	11	45 δ(CCH) + 15 ν(CC)
16	1154	1155	1163	25	16	30 δ(CCH) + 26 ν(CC) + 15 δ(CCC)
17	1114	1115	1114	1	6	42 δ(CCH) + 17 ν(CC) + 14 δ(CCC)
18	1058	1069	1053	2	30	37 δ(CCH) + 22 ν(CC) + 11 δ(CCC)
19	975	956	985	1	4	50 γ (CCCH) + 15 γ (CCCO) + 11 γ (CCCC)
20	-	-	943	0	0	36 γ (CCCH) + 18 γ (HCCH) + 10 γ (BrCCH)
21	881	893	876	4	15	32 δ(CCC) + 22 δ(CCH)
22	-	-	862	3	0	47 γ (CCCH) + 16 γ (HCCBr) + 13 γ (CCCC)
23	828	831	816	4	0	40 γ (CCCH) + 13 γ (OCCH) + 10 γ (CCCC) + 10 γ (BrCCH)
24	762	765	755	3	100	34 ν(CC) + 16 δ(CCC) + 16 δ(CCH)
25	-	-	749	29	2	52 γ (CCOH) + 10 γ (CCCH)
26	691	695	695	12	3	27 δ(CCC) + 15 δ(OCC) + 14 δ(CCH)
27	679	669	681	0	0	36 γ (CCCC) + 25 γ (CCCH) + 12 γ (CCCO)
28	611	626	611	6	8	33 δ(CCC) + 19 δ(CCCH) + 10 ν(BrC)
29	-	-	522	2	0	35 τ(CCCH) + 29 τ(CCCC) + 14 τ(CCCO)
30	-	-	450	2	27	38 δ(OCC) + 11 δ(CCC) + 11 δ(CCH)
31	-	-	422	0	0	33 τ(CCCC) + 27 τ(CCCH) + 16 τ(CCCO)
32	-	-	416	1	22	38 δ(CCC) + 14 δ(CCH) + 11 ν(CC)
33	-	-	318	0	14	21 γ (CCCO) + 20 τ(CCCC) + 14 τ(CCCH) + 10 τ(BrCCC)
34	-	-	281	2	7	27 δ(CCC) + 16 δ(BrCC) + 13 δ(OCC)
35	-	-	272	0	83	23 ν(BrC) + 27 δ(CCC) + 11 ν(CC) + 10 δ(CCH)
36	-	-	253	2	5	28 γ (CCCH) + 27 τ(CCCO) + 14 τ(CCCC)
37	-	-	166	1	39	36 δ(BrCC) + 21 δ(CCC)
38	-	-	135	0	21	28 τ(CCCC) + 19 τ(CCCO) + 16 τ(CCCH) + 15 τ(HOCC)
39	-	-	101	1	36	19 τ(CCCC) + 18 τ(CCCO) + 17 τ(CCCH) + 16 τ(BrCCC)

ν, stretching ; δ bending ; γ, out-of-plane bending ; τ, torsion. [a]The relative intensities of the FT-IR were normalized by equating the highest peak absorption to 100. [b]The relative intensities of Raman were normalized by equating the highest peak absorption to 100.

FMOs, IP and EA Properties and Chemical Reactivity Indices

The HOMO–LUMO, energy gap, ionization potential (*IP*) and electron affinity (*EA*) for 5BSA was computed using DFT-TD method B3LYP functional and 6–311 + + G(d,p) ground set. The calculated values are given in the Table 5. The parameters of *IP* and *EA* are intricately linked and pertain to the behavior of electrons within atoms or molecules. The technique of *IP* analysis was employed to determine the electronic structure.

Table 4. The calculated ^{1}H and ^{13}C NMR isotropic chemical shifts (in DMSO solvent, *ppm*) at the B3LYP/6-311++G(d,p) level of the mono, dimer, and trimer of 5BSA.

Atom	Experimental	Calculated (dimer)	Calculated (trimer)	Calculated (mono)
H15	10.92	9.77	8.99	12.27
H14	10.17	10.44	11.21	10.82
H11	7.65	7.93	7.88	8.54
H13	7.56	8.29	7.69	8.47
H12	6.93	7.23	7.61	7.89
C10	190.34	208.37	212.53	207.45
C5	160.37	157.84	157.84	173.58
C9	138.74	151.94	151.25	151.10
C6	131.14	150.78	148.49	147.64
C8	124.50	130.27	129.37	138.53
C4	120.25	127.18	128.02	130.74
C7	111.23	129.66	129.29	128,16

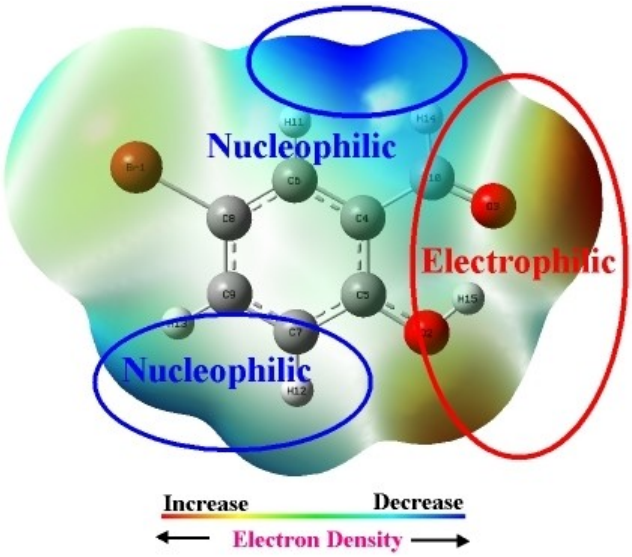

Figure 5. The Mep zone of 5BSA.

Table 5. The theoretically calculated some electronic and chemical properties of 5BSA. Units are eV.

E_{HOMO}	E_{LUMO}	E_{GAP}
−6.419	−2.189	4.230
Absolute hardness (η)	Chemical softness (S)	Reactivity index (ω)
2.109	0.474	4.379
Ionization potential (IP)	Electron affinity (EA)	Absolute electron negativity (χ)
8.451	1.033	4.304

The determination of the HOMO energy level is significantly influenced by *IP*, whereas the electronic characteristics of molecules are characterized by *EA*. The process of introducing an electron to a neutral atom or molecule in its gaseous form, leading to the creation of a negatively charged ion, is followed by the liberation of *EA* energy. Equations (1) and (2)[20] are used for the calculation of *IP* and *EA*.

$$IP = \left[E_0^+ - E_0\right] \quad (1)$$

E_0: The ground state energy refers to the lowest energy level in a neutral condition. E_0^+ and E_0^- are the energies of the cationic and anionic states, respectively, at the optimal geometry of the neutral molecule.

The 3D plots of the HOMO and LUMO orbitals are shown in Figure 6. The negative phase is depicted as green, whereas the positive phase is portrayed as red. It can be seen from Figure 6, that while the HOMO is localized on almost all molecules, the

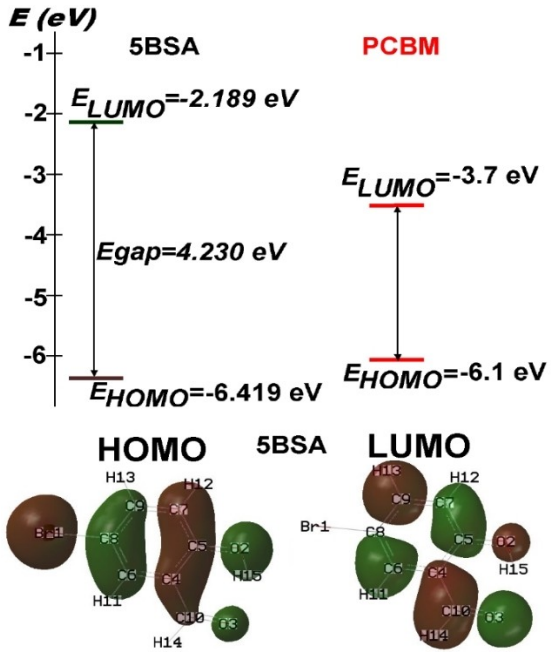

Figure 6. The HOMO and LUMO orbitals and energies of 5BSA and the acceptor PCBM.

Table 6. The experimental and calculated at the B3LYP/6-311++G(d,p) level UV-vis parameters for 5BSA.

Experimental λ_{max} (nm) (Ethanol)	λ_{max} (nm) (vacuum/ Ethanol)	Excitation energies (eV) (vacuum/Ethanol)
338.22	340.07/338.55	3.6459/3.6622
-	316.73/310.93	3.9145/3.9875
250.62	249.32/247.41	4.9729/5.0112
f (oscillator strengths) (vacuum/Ethanol)	***LHE*** (vacuum/Ethanol)	Major Contributes (vacuum/ Ethanol)
0.0546/0.0694	0.118/0.148	H>L (96%)/H>L (97%)
0.0003/0.0003	0.001/0.001	H-1>L (96%)/H-2>L (96%)
0.0000/0.0000	0.000/0.000	H>L+2 (97%)/H>L+2 (98%)

LUMO is localized on the salicylaldehyde. The energy gap is obtained at 4.230 eV. This band gap confirms 5BSA has very stable, charge transfer takes place within the molecule, and has bioactive nature.[25]

The maximum absorption wavelength is noted for the compound with gas and ethanol. The UV-absorption wavelength is available at 338 and 250 nm in the experimental spectrum due to the various transition of electrons. The more intense peak is at 338 nm. The oscillation strength (*f*) is a quantitative measure that represents the extent of electromagnetic radiation absorption or emission during transitions between energy levels of atoms or molecules. A greater magnitude of *f* will result in a higher degree of absorption. Another notable area of research is the examination of light-harvesting efficiency (*LHE*),[26] which is closely linked to *f*. Knowing that *f* is the oscillator strength corresponding to the maximum absorption wavelength (λmax), the parameter (LHE) can be determined as follows (Table 6) :

$$LHE = 1 - 10^{-f} \quad (3)$$

The experimental UV spectrum of 5BSA is compared with the simulated spectrum with ethanol solvents by Time-dependent density functional theory (DFT-TD) and B3LYP method as shown in Figure 7. Calculated results, (3.66 eV) 338.55 nm with oscillator strength $f = 0.0694$ for conformer 1 in ethanol are in good agreement with our experimental data.

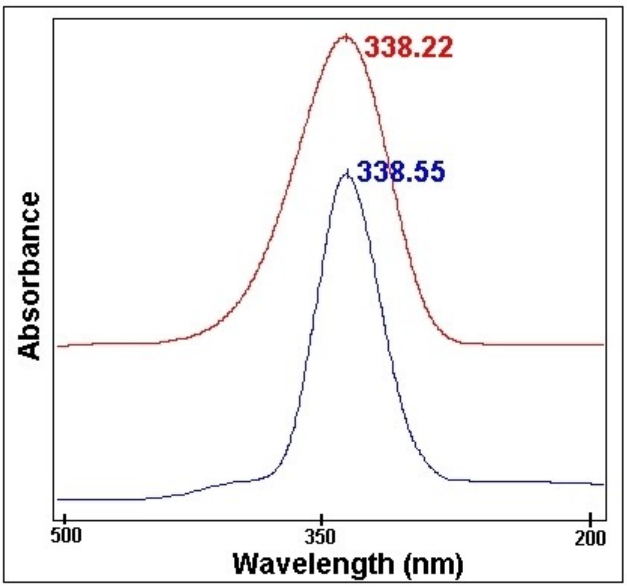

Figure 7. The Experimental in ethanol solvent and simulated at the B3LYP/6-311++G (d, p) level UV spectra of 5BSA molecule.

Density of States

Subsequently, a sequence of inquiries was carried out employing the DFT-TD/B3LYP methodology utilizing a 6–311++G (d, p) basis set. The analysis involved calculating the density of states (DOS). The evaluation of charge transport qualities involves analyzing the density of states, which has been accomplished using PyMolyze 1.1.[21] Understanding the density of states allows for the examination and analysis of the contribution of α and β electrons to the valence and conduction bands, respectively. However, the validity of DOS is contingent upon the electrons being unrestricted.[20] The degree of symmetry DOS of the molecule under investigation has been illustrated in Figure 8. The DOS analysis aligns well with the FMO results for the 5BSA molecule.

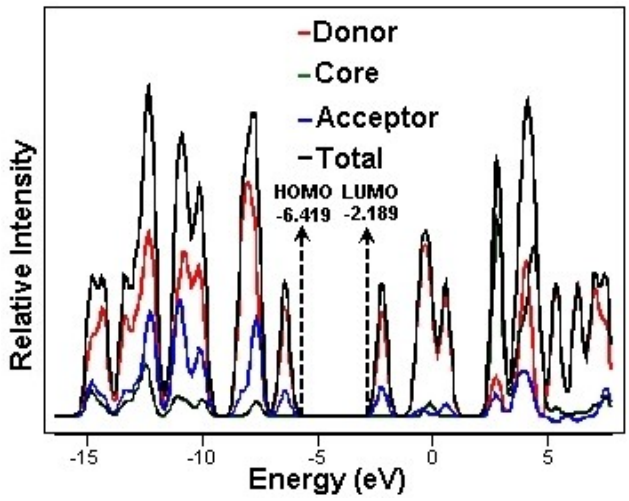

Figure 8. The visualization of DOS for the 5BSA molecule.

Photovoltaic Parameters

The open circuit voltage (V_{oc}) is a crucial characteristic that plays a major role in determining the productivity of a bulk heterojunction (BHJ) solar cell.[27] V_{oc} assesses the feasibility of electron injection from excited molecules to PCBM. An elevated LUMO energy in the acceptor and a reduced LUMO energy in the π-conjugated compounds often result in an increased V_{oc}, hence leading to improved solar cell performance. The value of V_{oc} may be determined using the Equation (3),[28] where E_{HOMO} (donor) represents the HOMO energy of the molecules being examined, E_{LUMO} (acceptor) represents the LUMO energy of PCBM, and 0.3 is the usual loss observed in BHJ organic solar devices.[29] The V_{OC} value of the 5BSA molecule is 2.42 eV. The findings imply that 5BSA exhibited an elevated potential difference across the solar cell, indicating improved charge separation and increased efficiency in converting light energy into electrical energy for 5BSA.

$$V_{oc} = ((|E_{HOMO(donor)}| - |E_{LUMO(acceptor)}|) - (0.3)) \quad (4)$$

In order to roughly predict the charge transfer behavior of organic materials, we performed calculations and analysis on the reorganization energies.[30] The lower reorganization energy supports faster electron transit. The calculation of hole reorganization energy (λ_h) and electron reorganization energy (λ_e) may be performed using Equations (4) and (5),[31] respectively. Furthermore, λ_{total} is defined as the sum of reorganization energy of the hole and those of the electron. The reorganization energies were computed utilizing the DFT method at the B3YLP/6-311++G(d,p) level of theory.

$$\lambda_h = \left(E_0^+ - E_+\right) + \left(E_+^0 - E_0\right) \quad (5)$$

$$\lambda_e = \left(E_0^- - E_-\right) + \left(E_-^0 - E_0\right) \quad (6)$$

The variables used in this context are as follows: E_0^+ represents the energy of a cation calculated using a neutral optimized structure, E_0^- represents the energy of an anion calculated using a neutral optimized structure, E_+ represents the energy of a cation calculated using a cation optimized structure, E_- represents the energy of an anion calculated using an anion optimized structure, E_+^0 represents the energy of a neutral molecule calculated using a cation optimized structure, E_-^0 represents the energy of a neutral molecule calculated using an anion optimized structure, and E_0 represents the energy of a neutral molecule at its ground state. The calculated value λ_h of 5BSA is 0.40977 eV, while the calculated value λ_e is 0.48446 eV and λ_{total} is also 0.89423 eV. In solar cells, the short-circuit current density J_{sc}[32] is often calculated as

$$J_{sc} = \int_{\lambda}^{0} LHE(\lambda)\Phi_{inject}\eta_{collect}d\lambda \quad (7)$$

where *LHE* is the light harvesting efficiency at a given wavelength, Φ_{inject} is the electron injection efficiency, and $\eta_{collect}$ is the charge collection efficiency. In order to gain a theoretical understanding of the relationship between J_{sc} and $\eta_{collect}$, we examined the *LHE*, Φ_{inject}, and λ_{total}. Until now, we calculated *LHE* (Table 5) and λ_{total}. Φ_{inject} is associated with the driving force (ΔG_{inject})[32] for electron injection from the photoinduced excited states of organic dyes to the semiconductor surface and it can be expressed as

$$\Delta G_{inject} = E^{dye^*} - E_{CB} \quad (8)$$

$$E^{dye^*} = E^{dye} - E_{exc} \quad (9)$$

Where E^{dye} is ($-E_{HOMO}$) *and* E_{exc} is excitation energy. Based on this formulation, E^{dye*} *is 2.7568* eV. By looking at the FMOs of the 5BSA molecule, we can find out how they behave as donors when they come into contact with TiO_2. We found that 5BSA is likely to add an electron to the semiconductor's conduction band when it is in the excited state by comparing its LUMO levels to the conduction band of TiO_2 (−4.00 eV). ΔG_{inject} is −1.2432 eV. The negative influence of ΔG_{inject} on the chosen dye indicates that the excited electron in the dye can easily avoid detection and go into the conduction band of TiO_2. This suggests that 5BSA can be useful in photovoltaic devices.

Evaluation TDM and Binding Energy

One important method for assessing the optical properties of organic molecule is by measuring the binding energy of its exciton (*Eb*). The energy required to generate free charges in the form of an electron or hole is determined by measuring the photon's energy and calculating the difference between the band gap and the first exciton transition state. It is denoted by Equation (10)[33].

$$E_b = E_{gap} - E_x \quad (10)$$

The 5BSA molecule has 0.5678 eV binding energy in ethanol phase. TDM is another excellent way for modeling exciton production, including its organization, mobility, and charge division. The DFT-TD technique B3LYP/6-311++G(d,p) is used to predict the absorption and emission of the molecules under study in the sixth excited state in ethanol. The corresponding diagrams can be seen in Figure 9.

TDM graphs in Figure 9 illustrate electron density on atoms and molecules based on the bottom horizontal axis and left vertical axis, respectively.

Conclusions

The equilibrium geometries, harmonic wavenumbers, ground state energy, and dipole moment of 5BSA were calculated for the first time. The FT-IR and Raman spectra of 5BSA were studied. The calculated vibrational values are in good agreement when they are compared with FT-IR and Raman experimental data. Gaussian[14] and Spartan[11] programs were

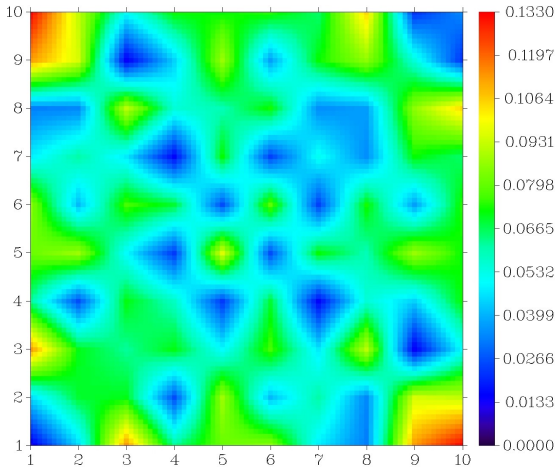

Figure 9. TDM map of 5BSA molecule.

used to find the most stable conformer of 5BSA. The structure of 5BSA compound was investigated both theoretically and experimentally as UV and (^{1}H and ^{13}C) NMR spectroscopy techniques. Moreover, the study of the HOMO-LUMO analysis at the DFT-TD and the MEP at the DFT method B3LYP/6-311++G(d,p) level in this work provides a valuable dataset for the researchers who work in the medicine and pharmacology fields. Furthermore, this paper discusses key characteristics closely related to J_{sc} such as *LHE*, E^{dye*}, ΔG_{inject}, and $\lambda_{total.}$ The study has examined reorganization energy, DOS, TDM, and E_b of 5BSA. Therefore, 5BSA is well-suited to serve as an electron donor in BHJ solar cells, whereas PCBM functions as the electron acceptor.

Conflict of Interests

The authors declare no conflict of interest.

Data Availability Statement

Research data are not shared.

Keywords: 5-BromoSalicylaldehyde · Spectroscopies · DFT approach · and Photovoltaic parameters.

[1] A. Mahmood, M. I. Abdullah, S. U.-D. Khan, *Spectrochim. Acta, Part A* **2015**, *139*, 425–430.
[2] A. Mahmood, M. I. Abdullah, M. F. Nazar, *Bull. Korean Chem. Soc.* **2014**, *35*, 1391–1396.
[3] X. Wu, F. Kang, W. Duan, J. Li, *Prog. Nat. Sci.: Mater. Int.* **2019**, *29*, 247–255.
[4] E. T. L. Fei, J. Biswas, B. Datta, D. Kumar, *Struct. Chem.* **2021**, *32*, 1973–1984.
[5] I. Borges Jr, R. S. S. Oliveira, M. A. S. Oliveira, *Theoretical and Computational Chemistry*, Vol. 22, Amsterdam: Elsevier **2022**, pp. 81–105.
[6] M. İ. Özgün, A. B. Batıbay, Ü. Bayram, Y. R. Eker, A. Terlemez, *Necmettin Erbakan Üniversitesi Fen ve Mühendislik Bilimleri Dergisi* **2023**, *5*, 1–8.
[7] N. Akdogan, M. Alp, A. Atilgan, A. Disli, Y. Erdogdu, A. Yildiz, *Mater. Lett.* **2023**, *351*, 135075.
[8] A. Frisch, J. Foresman, Pittsburgh PA: Gaussian Inc. **1996**, *302*, 3.2.
[9] D. Polo-Cerón, M. M. Hincapié-Otero, A. Joaqui-Joaqui, *Universitas Scientiarum* **2021**, *26*, 193–215.
[10] M. Ans, J. Iqbal, B. Eliasson, K. Ayub, *Comput. Mater. Sci.* **2019**, *159*, 150–159.
[11] Irvine, SPARTAN, Wavefunction, Inc., 18401, Von Karman Avenue, Suite 370, CA 92612 USA,2014 .
[12] T. A. Halgren, *J. Comput. Chem.* **1996**, *17*, 490–519.
[13] a) A. Becke, *Chem. Phys* **1998**, *98*, 5648; b) A. D. Becke, *Phys. Rev. A* **1988**, *38*, 3098–3100; c) A. D. Becke, *J. Chem. Phys.* **1993**, *98*, 5648–5652.
[14] M. J. T. Frisch, G. W.; H. B. Schlegel, G. E. Scuseria, M. A. Robb, J. R. Cheeseman, J. A. Montgomery Jr., T. Vreven, K. N. Kudin, J. C. Burant, J. M. Millam, S. S. Iyengar, J. Tomasi, V. Barone, B. Mennucci, M. Cossi, G. Scalmani, N. P., G. A. Rega, H. Nakatsuji, M. Hada, M. Ehara, K. Toyota, R. Fukuda, J. Hasegawa, M. Ishida, T. Nakajima, Y. Honda, O. Kitao, H. Nakai, M. Klene, X. Li, J. E. Knox, H. P. Hratchian, J. B. Cross, V. Bakken, C. Adamo, J. G., R. Jaramillo, R. E. Stratmann, O. Yazyev, A. J. Austin, R. Cammi, C. Pomelli, J. W. Ochterski, P. Y. Ayala, K. Morokuma, G. A. Voth, P. Salvador, J. J. Dannenberg, V. G. Zakrzewski, S. Dapprich, A. D. Daniels, M. C. Strain, O. M., D. K. Farkas, A. D. Rabuck, K. Raghavachari, J. B. Foresman, J. V. Ortiz, Q. Cui, A. G. Baboul, S. Clifford, J. Cioslowski, B. B. Stefanov, G. Liu, A. Liashenko, P. Piskorz, I. Komaromi, R. L. Martin, D. J. Fox, T. Keith, M. A. P., C. Y. Al-Laham, A. Nanayakkara, M. Challacombe, P. M. W. Gill, B. Johnson, W. Chen, M. W. Wong, C. Gonzalez, J. A. Pople, Gaussian, Inc., Wallingford CT, **2009**.
[15] R. Dennington, T. Keith, J. Millam, *Semichem Inc.: Shawnee Mission, KS* 2009.
[16] N. Sundaraganesan, H. Saleem, S. Mohan, M. Ramalingam, V. Sethuraman, *Spectrochim. Acta, Part A* **2005**, *62*, 740–751.
[17] Y. Atalay, D. Avcı, *Spectrosc. Lett.* **2008**, *41*, 116–121.
[18] S. Chtita, M. Ghamali, M. Larif, A. Adad, R. Hmammouchi, M. Bouachrine, T. Lakhlifi, *Int. J. Innov. Res. Technol. Sci. Eng.* **2013**, *2*, 7951–7962.
[19] M. U. Khan, M. Khalid, R. A. Khera, M. N. Akhtar, A. Abbas, M. F. ur Rehman, A. A. C. Braga, M. M. Alam, M. Imran, Y. Wang, *Arabian J. Chem.* **2022**, *15*, 103673.
[20] R. Iftikhar, R. Irshad, W. A. Zahid, W. Akram, R. A. Shehzad, S. A. Abdelmohsen, M. M. Alanazi, N. Shahzad, J. Iqbal, *J. Mol. Graphics Modell.* **2023**, *125*, 108588.
[21] N. M. O'boyle, A. L. Tenderholt, K. M. Langner, *J. Comput. Chem.* **2008**, *29*, 839–845.
[22] T. Lu, F. Chen, *J. Comput. Chem.* **2012**, *33*, 580–592.
[23] O. Dereli, Y. Erdogdu, M. T. Gulluoglu, *J. Mol. Struct.* **2012**, *1012*, 105–112.
[24] a) A. E. Segneanu, I. Gozescu, A. Dabici, P. Sfirloaga, Z. Szabadai, *Organic compounds FT-IR spectroscopy*, Vol. 145, InTech Rijeka, Croatia, **2012**; b) A. R. Raza, B. Nisar, M. Khalid, H. Y. Gondal, M. U. Khan, S. F. de Alcântara Morais, M. N. Tahir, A. A. C. Braga, *Spectrochim. Acta A Mol. Biomol. Spectrosc.* **2020**, *230*, 117995.
[25] D. Chen, H. Wang, *Proc. Combust. Inst.* **2019**, *37*, 953–959..
[26] A. Assyry, A. Hallaoui, A. Zarrouk, M. Hezzat, M. Assouag, S. Boukhris, M. Touhami, *Der Pharm. Chem.* **2015**, *7*, 128–138.
[27] X. He, L. Yin, Y. Li, *J. Mater. Chem. C* **2019**, *7*, 2487–2521.
[28] M. Raftani, T. Abram, N. Bennani, M. Bouachrine, *Res. Chem.* **2020**, *2*, 100040.
[29] M. C. Scharber, N. S. Sariciftci, *Prog. Polym. Sci.* **2013**, *38*, 1929–1940.
[30] K. M. Rosso, M. Dupuis, *Theor. Chem. Acc.* **2006**, *116*, 124–136.
[31] J.-D. Huang, K. Yu, X. Huang, D. Chen, J. Wen, S. Cheng, H. Ma, *IUCrJ* **2019**, *6*, 603–609.
[32] M. Bourass, A. T. Benjelloun, M. Benzakour, M. Mcharfi, M. Hamidi, S. M. Bouzzine, F. Serein-Spirau, T. Jarrosson, J.-M. Sotiropoulos, M. Bouachrine, *C. R. Chim.* **2017**, *20*, 461–466.
[33] R. Sikandar, A. Farhat, R. A. Khera, S. Jabeen, A. R. Ayub, P. Langer, J. Iqbal, *J. Mol. Graph. Modell.* **2021**, *106*, 107918.

Manuscript received: January 4, 2024